Observation of non-collisional ion heating in helical plasmas under dominant electron heating condition by neutral beam injection on LHD

K. Toi[#], S. Morita, K. Tanaka, A. Shimizu, M. Nishiura, K. Ogawa, N. Pablant^a, D.A. Spong^b, T. Tokuzawa, I. Yamada, M. Yoshinuma and LHD Experiment Team

National Institute for Fusion Science (NIFS), Toki 509-5292, Japan

- ^a Princeton Plasma Physics Laboratory, Princeton, New Jersey, USA
- ^b Oak Ridge National Laboratory, Oak Ridge, Tennessee, USA
- # Professor Emeritus of NIFS

E-mail: toi.kazuo@toki-fs.jp

Abstract

In LHD, significant increases in the central ion temperature T_{io} are observed in low density plasmas having a non-monotonic rotational transform profile produced by high energy neutral beam injection. The phenomena realize T_{io} $\sim T_{eo}$ (central electron temperature) under the strong electron heating condition. The T_{io} -increases disappear by a factor of two increase in electron density. During the T_{io} -increases, turbulent density fluctuations in the core plasma region are not suppressed but are enhanced slightly. The T_{io} -increases are caused by an addition of non-collisional ion heating, but not by confinement improvement due to reduction of turbulent transport. The ion heating power estimated from the T_{io} evolutions is much higher than the collisional ion heating by NBI. Ion Landau damping of standard GAM and coupled multiple GAM like modes induced by energetic ion driven geodesic acoustic modes (EGAMs) is the most likely candidate mechanism of the observed T_{io} -increases.

1. INTRODUCTION

In a future D-T burning plasma, energetic alpha particles dominantly heat electrons through the slowing down process. Bulk ions are heated via Coulomb collisions with electrons heated by alpha particles. For this reason, electron temperature T_e is usually higher than ion temperature T_i . In the past and present tokamak experiments, plasmas with $T_i > T_e$ show highly improved confinement because of a suppression of ion temperature gradient drift wave turbulence [1]. Therefore, high T_i is desirable for high fusion output, instead of high T_e . In a burning plasma, various auxiliary heating methods such as neutral beam injection (NBI) and radiofrequency (RF) waves heating are applied for ion heating in addition to plasma control. Alternative ion heating scenarios based on non-collisional processes are also studied theoretically. One of them is an idea called "alpha channeling" where direct energy transfer of alphas and energetic ions (EPs) to bulk ions using sophisticatedly designed waves is attempted to establish a path toward a hot-ionmode reactor [2,3]. The other interesting scenario is based on ion Landau damping of energetic ion driven geodesic acoustic modes (EGAMs) [4-6]. It is interesting and important to establish the non-collisional ion heating scenario for realizing a $T_i \gtrsim T_e$ plasma under dominant electron heating. In LHD, significant increases in the central ion temperature T_{io} are recently observed in low density plasmas having a non-monotonic rotational transform (ι-) profile produced by counter injection of high energy neutral beams. The phenomena have realized a $T_{io} \sim T_{eo}$ (central electron temperature) plasma

for the first time, under dominant electron heating condition by the NBI. This paper presents the details of the T_{io} -increase phenomena and discussions of the physics mechanisms. In Sec. 2, the experimental setup and plasma behaviors where the characteristic increases of ion temperature take place or do not are described. In Sec.3, possible candidate mechanisms of the T_{io} -increase are verified for consistency. In Sec.4, characteristics of energetic ion driven modes observed in the plasmas are described. In Sec.5, the additional ion heating power density is estimated by a simple power balance of bulk ions. In Sec.6, likely mechanisms of the observed non-collisional ion heating are discussed. This paper is summarized in Sec.7.

2. Experimental setup and plasma behaviors

In this experimental campaign, plasmas are produced in the magnetic configuration that the magnetic axis position in the vacuum is $R_{ax}=3.75$ m at low toroidal field B_t =1.3-1.4 T. In order to modify the *t*-profile considerably, tangential NBIs with ~140 keV hydrogen beams are injected in the counter direction to reduce the rotational transform generated by external coils. A small amount of neon is puffed to minimize an electron return current by raising the effective charge of $Z_{eff} \sim 4$ to 5, so large toroidal plasma current is driven by NBI up to ~150 kA. Line averaged electron density is adjusted in low density range less than 1x1019 m-3 to achieve higher beam ion beta for strong drive of EGAMs and maintain an anisotropic distribution function of EPs. On the plasma conditions, a reversed magnetic shear (RS) configuration is produced. The rotational transform profile has an off-axis minimum ι_{min} at $\rho \sim 0.5$ (ρ : normalized minor radius). The reversed magnetic shear Alfven eigenmodes (RSAEs) were identified by comparison of the observed frequency and radial mode location with the numerical calculations [7],

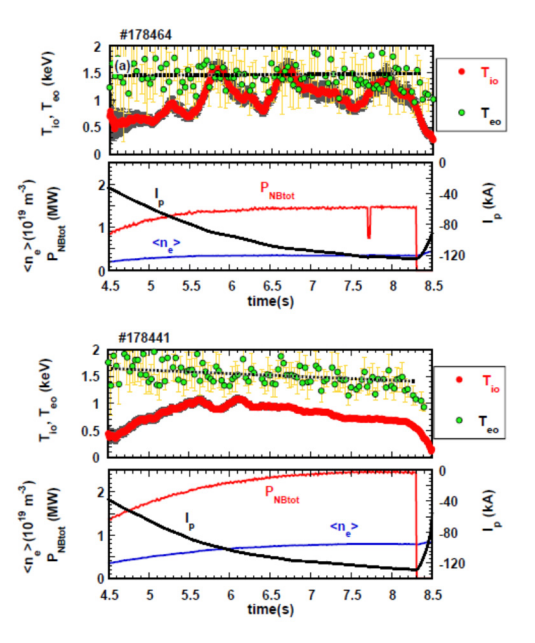


Fig.1 Time evolutions of the central ion and electron temperatures (T_e , T_i), the line averaged electron density (<n $_e>$), total absorbed NBI power (P_{NBtot}) and NB-driven plasma current (I_p) in low (#178464) and higher (#178441) density plasmas. The T_{eo} data (green circles) are obtained by Thomson scattering, and the time-average is indicated with a solid line among the data points.

where the ι -profiles measured by the motional stark effect diagnostic (MSE). Since the MSE is not applicable in the present experiment, the main parameters of the RS ι -profile are predicted by the technique of the Alfven spectroscopy with help of the observed RSAE and the global Alfven eigenmode (GAE) frequencies [8]. The central ion temperature T_{io} is obtained reliably from the Doppler broadening of the ArXVII spectral line by a crystal spectrometer, where a tiny amount of argon is doped in a plasma [9]. For limited shots, the radial profiles of ion temperature were measured by an X-ray imaging crystal spectrometer (XICS) [10]. Microturbulence density fluctuations in the plasma core region are monitored by a CO₂ laser phase contrast imaging. Radial profiles of plasma potential fluctuations and stationary potential are measured by a heavy ion beam probe (HIBP). Rapid electron temperature changes and the fluctuations are monitored with an electron cyclotron emission (ECE) spectrometer.

NBI absorbed power are shown for two typical shots having low ($< n_e > \sim 0.35 \times 10^{19} \text{ m}^{-3}$) and high $(\langle n_e \rangle \sim 0.8 \times 10^{19} \text{ m}^{-3})$ density. In the low density shot, intermittent increases in T_{io} are observed, while T_{io} in the high density shot evolves smoothly without the characteristic increases. The T_{io} increases realize a plasma of $T_{io} \sim T_{eo}$ under dominant electron heating. Note that the NBI absorbed power in the high density shot is by about 1.7 times higher than that in the low density one. The ion temperature profiles were measured by the XICS diagnostic in the similar shot with the T_{io} increase in the past campaign, as shown in Fig.2. The fairly flat ion temperature profile evolves to a centrally peaked one, while electron temperature and density profiles remain unchanged during the T_{io} increase.

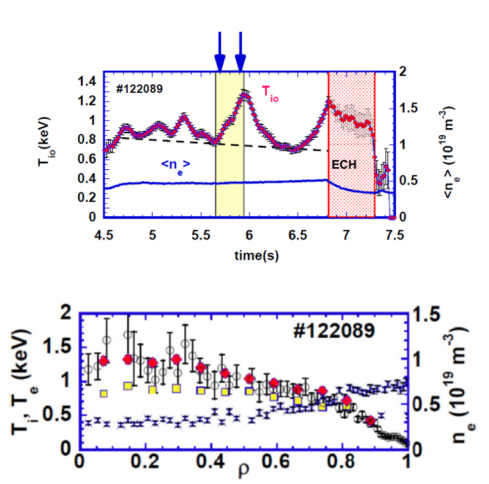


Fig.2 T_i radial profiles measured by the XICS at two time slices indicated with the arrows in the upper traces, together with T_e and n_e -profiles. The T_{io} evolution is obtained by a crystal spectrometer.

3. Possible physics mechanisms of the ion temperature increases

Following mechanisms are thought as possible candidates of the T_{io} -increases: (1) Ion confinement improvement due to suppressed microturbulence, (2) transition of the neoclassical transport in a helical plasma from "ion root" to "electron root", and (3) addition of ion heating by non-collisional processes. The candidate (1) can be checked by the correlation between the T_{io} -increases and the temporal behaviors of microturbulence density fluctuations in the plasma core region, since the ion temperature increase takes

place in the plasma core region of $\rho \lesssim 2/3$ as seen from Fig.2. In Fig.3(a), time evolutions of T_{io} and microturbulence density fluctuation amplitude integrated over the plasma core region of $\rho \lesssim 2/3$ are shown for the low density shot. The fluctuation amplitude increases noticeably during each Tioincrease phase, and quickly decays just after the phase. Moreover, Hα emission shown in Fig.3(b) is noticeably enhanced during the T_{io} -increase, while the line averaged electron density remains unchanged. This indicates the degradation of particle confinement. It is concluded from the time behaviors of microturbulence and Hα emission that the T_{io} -increases are not caused by the ion confinement improvement. The above phenomena have a marked difference with a typical observation of ion temperature increases due to suppression of microturbulence in LHD [11]. For the candidate (2), when neoclassical transport from

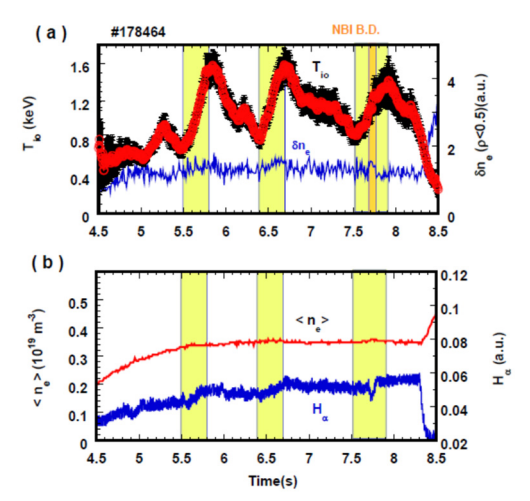


Fig. 3(a) Time behaviors of turbulent density fluctuation amplitude and T_{io} . (b) Time evolution s of line averaged electron density and H α emission. Each T_{io} -increase phase is highlighted with a yellow zone. Note that the NBI power breaks down in the interval from t~7.7s to 7.8s.

the so-called "ion root" characterized with nearly zero or negative radial electric field E_r is changed to the "electron root" with positive radial electric field, particle and energy transport of ions should be reduced considerably. Actually, in LHD the ion temperature increase due to reduction of the ion thermal diffusivity was observed in the transition to the electron root in the plasma peripheral region with high helical ripple [12]. In the present plasma shots, however, the stationary plasma potential profile has a shallow convex structure in the central region, that is, $E_r \leq 0$. The plasma shots are in the ion root regime, so the transition to the electron root does not take place. The candidate mechanisms (1) and (2) are ruled out. In conclusion, the observed T_{io} -increases are caused by an addition of non-collisional ion heating power to the low collisional ion heating by NBI. At present, ion heating via ion Landau damping of EGAM is thought to be the most likely for the observed T_{io} -increases in the RS plasmas obtained on the present experimental condition.

4. EGAMs and characteristic Alfven eigenmodes destabilized by counter NBIs

The pitch angle distribution of energetic ions (EPs) generated by tangential NBIs has a peak at $\Lambda_o \sim 0.125$ and the width $\Delta \Lambda \sim 0.175$, where the distribution is assumed to be a form of exp[- $\{(\Lambda - \Lambda_o)/\Delta\Lambda\}^2$ with the pitch parameter $\Lambda =$ $\mu B/E$, where μ , B and E are respectively the magnetic moment, total magnetic field strength and particle energy. In the low density shot shown in Fig.1, the deflection time of EPs is comparable to the NBI pulse duration of 5 s. The t-profiles in a net current free LHD plasma have a monotonic convex shape. Counter current drive by NBIs in a neon doped plasma can produce a reversed magnetic shear t-profile having an off-axis minimum ι_{min} in the R_{ax} = 3.75 m configuration. Characteristic RSAEs having m=3/n=2, m=2/n=1 and m=3/n=1 are excited sequentially in time by EPs, as seen from the spectrogram of magnetic fluctuations shown in Fig.4(a), where m and n stand for poloidal and toroidal mode numbers, respectively. The RSAE frequency is swept in

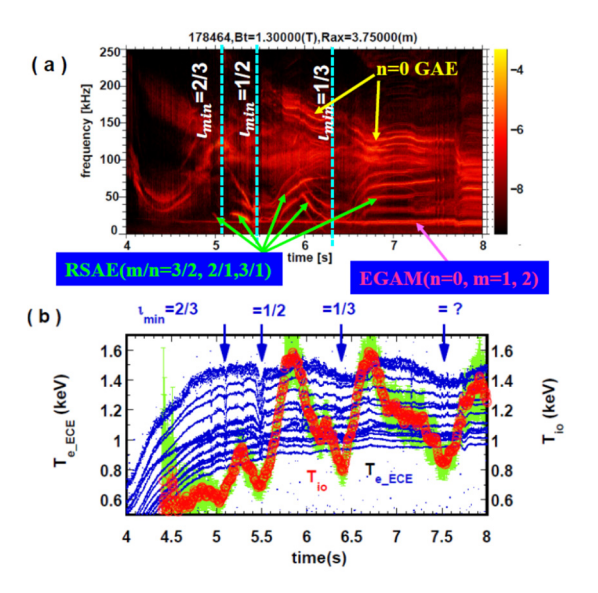


Fig.4(a) Spectrogram of poloidal magnetic fluctuations, where EGAM, RSAEs and n=0 GAEs are identified. (b) Time evolution of T_{io} and electron temperatures T_{e_ECE} measured at R=3.87-4.33m by an ECE spectrometer. The times of $\iota_{min}=2/3$, 1/2 and 1/3 are indicated by vertical broken lines and arrows.

time, responding to the temporal evolution of the ι -profile. The frequency takes the minimum at the time that ι_{min} passes the rational values, i.e., 1/2 or 1/3. In the shots, the n=0 GAEs are also detected at around 200 kHz and the frequencies decrease to ~ 100 kHz at the plasma current peak. The observed frequency agrees well with the eigenfrequencies calculated by the AE3D code [13]. The frequency is in proportion to the $\iota(0)$, but is insensitive for the changes in ι_{min} . Reliable information about $\iota(0)$ and ι_{min} is obtained from the observed frequencies of RSAE and ι =0 GAE. In low frequency range less than \sim 20 kHz, an ι =0 magnetic fluctuations having nearly constant frequency is strongly excited during the counter NBIs. The mode has a standing wave structure poloidally with ι =2. The mode having the ι =1

structure begins to rotate poloidally in the latter phase of the plasma. Moreover, this mode accompanies with large amplitude potential fluctuations of the order of ~ 1 kV. The mode frequency of the observed EGAM is about half of the standard GAM frequency. The n=0 mode shows the characteristic features of EGAM clearly [14]. More importantly, the frequency does not respond to the T_{io} increase, as seen from Fig.4(a) (and also Fig.5(c) shown below). The EGAM and GAEs with n=0 observed in the RS plasmas are destabilized by the positive gradient in the velocity space due to an anisotropic distribution function as mentioned above. Strong mode couplings between EGAM and RSAEs, and also EGAM and n=0 GAEs

generate a multitude of coupled modes, as seen from Fig.4(a). In Fig. 4(b), the time evolutions of T_{io} and electron temperature. T_{e_ECE} at several radial positions measured by the ECE spectrometer are compared with those of the mode frequencies of RSAE, n=0 GAE and EGAM. Each strong T_{io} increase starts just after the time that ι_{min} passes the rational values such as 1/2 and 1/3. Note that the T_{e_ECE} data in the central region show small and but sharp dips at the times of $\iota_{min} = 1/2$ and 1/3. These dips may be induced by double tearing modes (DTMs) in a current carrying helical plasma, since the stability index of tearing modes, $\Delta'(0)$ at two rational surfaces are positive, that is, the DTMs are unstable [15, 16]. The RSAEs, n=0 GAE and EGAM are also excited in the high density plasma shown in Fig.1. However, the $\iota(0)$ decreases more quickly than the low density one.

The time evolution of the EGAM amplitude and the radial profiles are measured successfully in some shots, by applying the 10 Hz radial sweeping of the HIBP probe beam. The EGAM potential profiles are obtained every 0.05 s. Time evolution of the rootmean squared amplitude of the EGAM potential fluctuations ϕ_{rmsEG} is shown in Fig.5(b), which are derived from the traces of the profiles near the plasma center $\rho \lesssim 0.2$. This figure is compared with the time evolutions of T_{io} (solid circles) and $T_{io\ col}$ (broken curve) predicted for the condition with only collisional ion heating, in Fig.5(a). Moreover, the evolutions of $\iota(0)$ and ι_{min} predicted from the AE frequencies are shown together with the observed EGAM frequency in Fig.5(c). Figure 5(d) shows the evolutions of magnetic fluctuation amplitude of RSAEs. As seen from Fig.5(b), the ϕ_{rmsEG} exceeds ~ 1 kV and decreases clearly

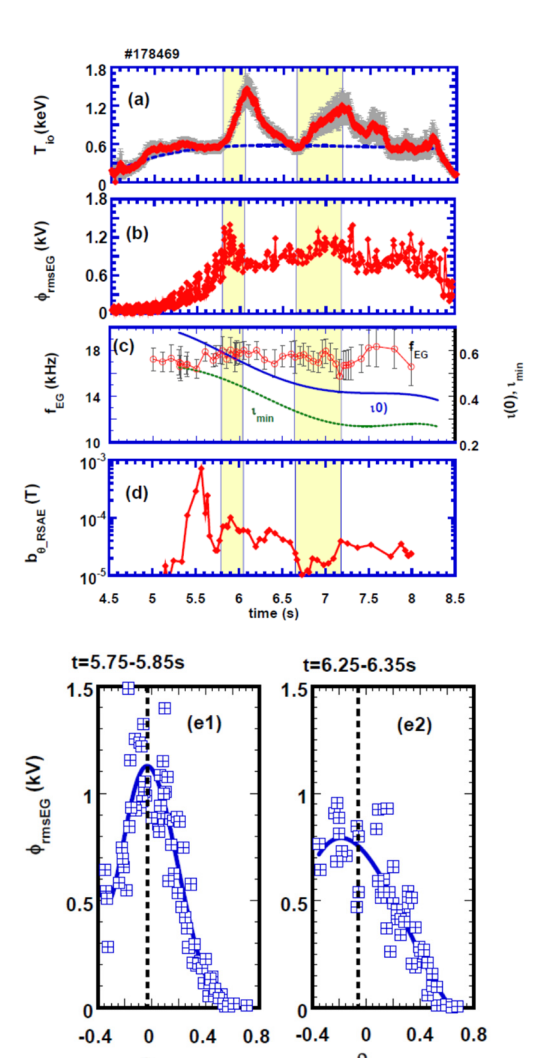


Fig. 5 Time evolutions of (a) T_{io} and T_{io_col} , (b) the root-mean-squared EGAM amplitude ϕ_{rmsEG} , (c) $\iota(0)$, ι_{min} and the EGAM frequency with the spectral width, and (d) the RSAE amplitude. The T_{io} -increase phases are highlighted with the yellow bands. Radial profiles of ϕ_{rmsEG} just before (e1) and after (e2) the T_{io} -increase Phase.

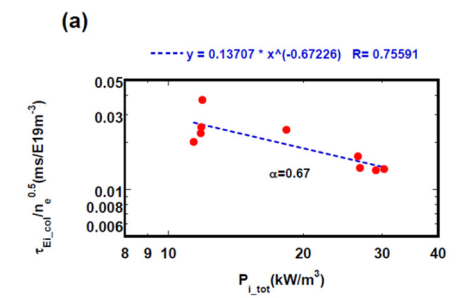
during the T_{io} -increase phase. The T_{io} -increases take place in the upward sweeping phase of the RSAE frequency.

5. Estimation of additional ion heating power density from the time evolution of T_{io}

Using the data T_{io} and T_{io_col} shown in Fig.5(a), the additional ion heating power density can be estimated from the following simple power balance of bulk ions, taking into account of the power degradation in the ion energy confinement time as $\tau_{Ei} \propto P_{itot}^{-\alpha}$, where $P_{itot} = \langle p_{NBi} \rangle + \langle p_{ei} \rangle + \langle p_{iadd} \rangle$ and α is a positive parameter. That is,

$$\langle \frac{dw_i}{dt} \rangle + \langle w_i \rangle / \tau_{Ei} = \langle p_{NBi} \rangle + \langle p_{ei} \rangle + \langle p_{iadd} \rangle$$
 (1)

Three terms in the right-hand side of eq.(1) are respectively the volume-averaged power density of the collisional ion heating by NBI, that from electron to ion through collisions and a predicted non-collisional ion heating. Here, $\langle w_i \rangle = w_i(0) f_{prof_wi}, \langle p_{NBi} \rangle = \frac{P_{NBi}}{V}$ and $\langle p_{ei} \rangle = p_{ei}(0) f_{prof\ ei}$, where V is the plasma volume. The parameters f_{prof_wi} and f_{prof_ei} are the profile shape factors estimated from the T_i , T_e and n_e radial profiles. In the case $\langle p_{iadd} \rangle = 0$, the other terms in eq. (1) are evaluated using the experimental data shown in Fig.5(a), except the T_{io} is replaced with T_{io_col} . In this shot, the averaged electron density is $\langle n_e \rangle = 0.33 \times 10^{19} \text{ m}^{-1}$ ³. In the case τ_{Ei} is replaced with τ_{Ei_col} . The power degradation of $\tau_{Ei\ col}$ has been crudely estimated using the data of $T_{io\ col}$ and other experimentally obtained data, as shown in Fig. 6(a). From the least-square fitting, $\tau_{Ei\ col}/n_e^{0.5}$ is in proportion to $P_{itot}^{-0.67}$. The results indicate a slightly stronger power degradation for the ISS04 scaling of the global energy confinement time [17]. In Fig.6(b), time evolutions of the additional ion heating power density estimated by eq.(1) are shown for α = 0.6 same as the ISS04. A weaker degradation case of α = 0.3



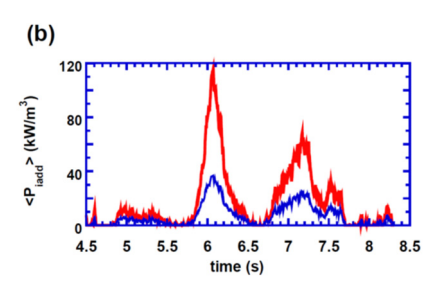


Fig. 6 (a) Dependence of ion energy confinement time on total ion heating power density on assumption of the same density dependence as the ISS04, (b) Additional non-collisional ion heating power density for the degradation of α =0.6 (red curve). The power density at the α =0.3 case is also shown with a blue curve in Fig. (b) for the comparison.

is also shown for the comparison. The calculated values of $< p_{iadd} >$ results are nearly independent of the profile shape factors, while they sensitively depend on α . The $< p_{iadd} >$ for α =0.6 reaches the range of 50–80 kW/m³ in all shots that clear T_{io} -increases are observed, which is much higher than the collisional ion heating power by NBIs ($\le 10 \text{ kW/m}^3$).

6. Discussions

In the initial growing-phase of EGAM, the $\iota(0)$ is ~0.65, i.e., low q(0) ~1.5 and T_{eo}/T_{io} ~2.5. Noticeable

damping rate of GAM is expected and the related ion heating might be triggered in the T_{io} -increase phase. The observed EGAM potential fluctuations decrease obviously, but stay a finite value during the first increase phase of T_{io} , as seen from Fig.5(b). The EGAMs might be damped as same as the standard GAMs in a helical plasma [18, 19]. As mentioned in Sec.4, however, the observed EGAM frequency is about half of the GAM frequency derived by a gyrokinetic theory [18]. Moreover, the frequency is nearly independent of the T_{io} -increases, as seen from Figs.4(a) and 5(c). The real part of the normalized complex angular frequency $\widehat{\omega}_r$ defined as the ratio of the wave phase velocity to the ion thermal velocity is in the range of ~1.5 to

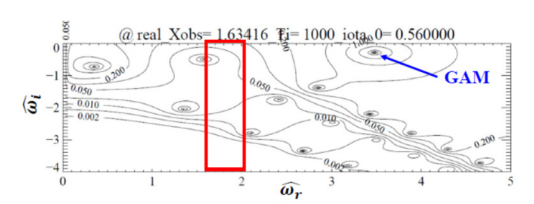


Fig. 7 Contour plot of the $1/F_{dis}(\widehat{\omega})$ on the complex variables plane for the experiment conditions: T_i =1.0 keV, T_e =1.5 keV, $\iota(0)$ =0.56, the EGAM frequency= 17 kHz, R=3.75 m and k_r =8 m⁻¹. There are many poles corresponding to eigenmodes which can respond to EGAM. The standard GAM is indicated with an arrow, where the damping rate is small as $\widehat{\omega}_r$ >> $\widehat{\gamma}_d$. The red frame indicates the predicted range of $\widehat{\omega}_r$ for the observed EGAM, since the q value varies over the EGAM profile.

~2.5 for the experimental data. The normalized damping rate $\hat{\gamma}_d$ estimated simply by an analytic equation in ref. [18] is comparable or larger than $\widehat{\omega}_r$. Therefore, the equation is not applicable to the estimation of the EGAM damping rate. Instead, the GAM dispersion relations $F_{dis}(\widehat{\omega})$ given in ref. [18] should be solved by a full complex analysis. In Fig.7, the magnitude of $1/F_{dis}(\widehat{\omega})$ is plotted on the complex plane of $\widehat{\omega}$ for the experiment parameters. The effect of the finite orbit width effects can be neglected because of low k_r (=8 m⁻¹). Moreover, the helical field effects slightly enhance the damping rate for that in a tokamak. Many peaks corresponding to the standard GAM and GAM like modes are found in Fig.7. Certainly, the real part $\hat{\omega}_r$ for the standard GAM is ~3.5, and the normalized damping rate $\hat{\gamma}_d$ is 0.30. The result of $\widehat{\omega}_r \gg \widehat{\gamma}_d$ indicates the typical character of the GAM. On the other hand, the $\widehat{\omega}_r$ evaluated for the observed EGAM frequency is ~ 1.63, and does not hit the pole of the GAM. In this situation, the EGAM oscillations can be regarded as an external wave source. The function $1/F_{dis}(\widehat{\omega})$ corresponds to the response function of the electric field fluctuations to the external radial current density induced by EGAM [19]. Many GAM-like multi-modes having large damping rates may effectively interact with the EGAM oscillations through nonlinear mode coupling among them, and absorb the EGAM wave energy. Thus absorbed energy may be transferred to bulk ions via ion Landau damping. In the present shots where the EP pressure is by a factor of 10 higher than the bulk plasma pressure, large growth rate γ_h of EGAM is expected [14]. Loss cone due to helical ripple and/or charge-exchange losses in low density plasma may further enhance the growth rate, so the situation $\gamma_h \gtrsim \gamma_d$ may be realized as in the experiment. So far, the rapid decay following the T_{io} -increase phase is not fully understood. The second T_{io} -decay shown in Fig.5(a) synchronizes with the re-enhancing phase of the RSAE activities shown in Fig.5(d). The enhanced RSAE may facilitate the radial transport of the EP density, and suppress the EGAM

activities noticeably. However, the correlation between the first decay of T_{io} and the RSAE activities is unclear. The phase overlaps with the unstable phase of strong m=2 DTM. The m=2 DTM may play a role in the first decay. Microturbulence fluctuations, of course, have no correlation with the decay, as seen from Fig.3. The quantitative estimation of the ion heating power caused by the EGAM damping and the understanding of the characteristic decay following the significant T_{io} -increases are left for the future important research targets.

7. Summary

In low density plasmas sustained by high beam pressure, strong and intermittent increases in T_{io} have been observed with good reproducibility. The T_{io} -increases do not result from improved confinement due to suppression of microturbulence but rather enhance turbulent fluctuations and H α emission. Under the same power degradation in the ion energy confinement time with the ISS04 scaling, the T_{io} -increases correspond to an addition of large non-collisional ion heating power in the range of ~50-80 kW/m³, much higher than the collisional one (~10 kW/m³) by NBI. Correlation between the T_{io} -increase and the EGAM potential fluctuation amplitude is clearly observed. The quantitative evaluation of the non-collisional ion heating power density by EGAM is left for the future important research target.

Acknowledgements

Prof. H. Sugama and Prof. T. Watari are acknowledged for stimulated discussions about GAMs. The authors thank other members of the LHD experiment and operation teams for their supports. This research was in part supported by NIFS21KLPH048.

References

- [1] Doyle, E.J., Houlberg, W.A., Kamada. et al., Nucl. Fusion 47 (2007) S18.
- [2] Fisch, N.J. and Rax, J.M., Phys. Rev. Lett. 69 (1992) 612.
- [3] Fisch, N.J. and Herrmann, M.C., Plasma Phys. Control. Fusion 41(1999) A221.
- [4] Sasaki, M., Itoh, K. and Itoh, S-I., Plasma Phys. Control. Fusion 53 (2011) 085017
- [5] Wang H., Todo Y., Osakabe, M., Ido, T. et al., Nucl. Fusion 59 (2019) 096041.
- [6] Nobikau, I., Biancalani, A., Bottino, A. et al., Phys. Plasmas 27 (2020) 042512.
- [7] Toi, K, Watanabe, F., Tokuzawa. T. et al., Phys. Rev. Lett. 105 (2010) 145003.
- [8] Gorelenkov, N.N., Pinches, S.D. and Toi, K., Nucl. Fusion 54 (2014) 125001, and references therein.
- [9] Morita, S. and Goto, M., Rev. Sci. Instrum. 74 (2003) 2375.
- [10] Pablant, N.A., Bitter, M., Delgado-Aparicio, L. et al., Rev. Sci. Instrum. 83 (2012) 083506.
- [11] Du X.D., Toi, K., Osakabe, M., Ohdachi, S. et al., Phys. Rev. Lett. 114 (2015) 155003.
- [12] Ida, K., Funaba, H., Kado, S. et al., Phys. rev. Lett. 86 (2001) 5297.
- [13] Spong, D.A., D'Azevedo, E. and Todo, Y., Phys. Plasmas 17 (2010) 022106.
- $[14]\ Fu, G.Y., Phys.\ Rev.\ Lett.\ {\bf 101}\ (2008)\ 185002.$
- [15] Furth, H.P., Rutherford, P.H. and Selberg, H., Phys. Fluids 16 (1973) 1054.
- [16] Matsuoka, K., Miyamoto, K., Ohasa, K. et al., Nucl. Fusion 17 (1977) 1123.
- [17] Yamada, H., Harris, J.H., Dinklage, A. et al., Nucl. Fusion 45 (2005) 1684.
- [18] Sugama, H., and Watanabe, T.H., Phys. Plasmas 13 (2006) 012501 and 14 (2007) 079902.
- [19] Watari, T., Hamada, Y., Notake, T. et al., Phys. Plasmas 13 (2006) 062504.